Supplementary Information

Gorvin et al. 10.1073/pnas.1302063110

SI Materials and Methods

Primary Cell Culture and Immortalization. Primary cell cultures were established from morning first voided urine samples and maintained in supplemented DMEM-F12 HAMS medium (Gibco), at 37 °C, in 5% (vol/vol) CO_2, as described (1, 2). Cells were immortalized by infection with SV40-T (U19tsA58) and human telomerase reverse transcriptase (hTERT), and grown at 33 °C, 5% (vol/vol) CO_2 until confluent, by using methods described (3). Proximal tubule cells were isolated from cell populations by fluorescence-activated cell sorting (FACS) using mouse–anti-human CD13-FITC antibody (Dako) (1:100 dilution in PBS). CD13-positive cells were immediately seeded on NIH 3T3 (ATCC, LGC Standards) fibroblast feeder layers and grown for ∼12 d. Colonies were picked by using cloning discs (Sigma-Aldrich) soaked in trypsin/EDTA, seeded into new flasks, and grown to confluency.

Flow Cytometry. Confluent subcloned cells were seeded in six-well plates, trypsinized, and single cell suspensions were treated with CD13-FITC (1:100 dilution in PBS) (Dako) before investigation by flow cytometry (1). Unlabeled cells were used as negative controls. Data were gathered by using Cytomation Summit (version 3.0) and analyzed by using FlowJo (version 9.0.2) software (4).

Mutational Analysis. DNA was extracted from peripheral leukocytes and conditionally immortalized proximal-tubular epithelial cell lines (ciPTECs) by using Gentra Puregene Blood Kit (Qiagen) and used for PCR amplification of the coding region exons and intron-exon boundaries of *CLCN5* (primer sequences available on request) as described (5). The DNA sequences of the PCR products were determined by using DYEnamic ET Terminators (Amersham Biosciences) and the ABI377 semiautomated sequencer (Applied Biosystems) (6).

RT-PCR and Quantitative RT-PCR Analysis. First-strand cDNA was generated from 1 μg of total RNA from each cell line extracted by MirVana (Ambion), using Quantiscript reverse transcriptase in the Quantitect Reverse Transcription kit (Qiagen) (7). PCR was performed on cDNA by using primers specific for ATP-binding cassette family member multidrug resistance protein 4 (*ABCC4*), ATP-binding cassette sub-family B member 1, P-glycoprotein (*ABCB1*), Na+K+Cl- cotransporter-2 (*NKCC2*), K+ inwardly-rectifying channel, subfamily J, member 1 (*KCNJ1*), Calbindin-1 (*CALB1*), Transient receptor potential cation channel, subfamily V, member 5 (*TRPV5*), Uroplakin-IIIA (*UPKIIIA*), Calmodulin (*CaM*), Cubilin (*CUBN*), Megalin, also referred to as Low-density lipoprotein related protein 2 (*LRP2*), Kinesin family member 3B (*KIF3B*), V-ATPase subunits A2 (*ATP6V0A2*) and D (*ATP6V1D*) and Cyclin D1 (*CCND1*) (primer sequences available on request), as described (8). Human kidney RNA (Clontech) and bladder RNA (extracted from ATCC CRL-1473 cells) were used as controls. Quantitative RT-PCRs (qRT-PCRs) were carried out by using the Rotorgene Sybr Green Kit (Qiagen) in triplicate in four independent samples for each ciPTEC using a Rotorgene 5 (Qiagen), as described (9). All qRT-PCR test samples were normalized to levels of the geometric mean of three reference genes, *GAPDH, CCND1,* and *CCND2*. Threshold cycle (C_T) values were obtained from the start of the log phase on Rotorgene Q Series Software, and C_T values were analyzed in Microsoft Excel 97–2010 by using the Pfaffl method (10). Data for each ciPTEC was normalized to the control ciPTEC.

Western Blot. Protein was extracted from confluent cell lines by using RIPA buffer (50 mM Tris at pH 7.4, 150 mM NaCl, 1% (vol/vol) Igepal CA630, 0.5% Na^+-deoxycholate, 0.1% SDS, 0.01% phenylmethane sulphonylfluoride, 3% (wt/vol) aprotinin and 1 mM Na-orthovanadate), eluted in Laemmli buffer, and analyzed by Western blotting using 12% (vol/vol) sodium-dodecyl sulfate polyacrylamide gel electrophoresis (SDS/PAGE) (11). Following transfer to polyvinylidene difluoride membrane (Amersham), blots were probed with rabbit anti-AQP1 (1:2,000; Chemicon International, Millipore), goat–anti-AQP2 (1:250; Santa Cruz), rabbit–anti-TRPV5 (1:250; Santa Cruz), rabbit–anti-UPKIIIA (1:500; Abcam), rabbit–anti-chloride channel-5 (CLC-5) (1:200; Sigma-Aldrich), or rabbit–anti-α-tubulin (1:2,000, Abcam), and HRP-conjugated secondary antibodies goat–anti-rabbit (1:3,000; Bio-Rad) or donkey–anti-goat (1:3,000; Bio-Rad) (11). Blots were visualized by using Pierce ECL Western blotting substrate (Thermo Fisher Scientific) on a Bio-Rad Chemidoc XRS+ system (12).

Confocal Imaging. Confluent ciPTECs were plated in six-well plates containing poly-L-lysine–treated coverslips and cultured at 37 °C for 7–10 d (13). For Z-stack imaging, cells were fixed in ice-cold methanol and coimmunostained with rabbit polyclonal anti–ZO-1 (Invitrogen) and mouse monoclonal anti-microtubule-associated protein, RB/EB family, member 1 (MAPRE1) (EB-1; Abcam), and secondary antibodies anti-rabbit Alexa Fluor 488 and anti-mouse Alexa Fluor 594 (Molecular Probes), respectively (13). For megalin localization studies, cells were incubated in serum-free media, before exposure to 5 mg/mL unlabeled albumin, fixed in 4% paraformaldehyde/PBS, permeabilized in 1% Triton X-100/PBS, and immunostained with primary goat–anti-megalin (Santa Cruz) and secondary anti-goat Alexa Fluor 594 antibodies. The images and Z stacks were recorded by using a confocal laser-scanning microscope (Zeiss, LSM 10 META) with a Plan-Achromat 63×/1.4 N.A. oil differential interference contrast (DIC) objective (13). An argon laser $\lambda = 488$ nm was used to excite Alexa Fluor 488 fluorescence and a HeNe laser $\lambda = 543$ nm for Alexa Fluor 594 (13). Emission of Alexa Fluor 488 and Alexa Fluor 594 was detected in the Multi-track mode in META channels of the confocal system within the following spectral detection ranges: from 509 to 550 nm for Alexa Fluor 488, and from 580 to 620 nm for Alexa Fluor 594 as described (13). Images were merged and orthogonal sections were analyzed by using Zeiss LSM Image browser software (13).

Confocal images were also collected from live HEK293 cells transiently transfected with wild-type (WT) or mutant p-enhanced yellow fluorescent protein (pEYFP)–CLC-5 constructs and seeded onto Fluorodishes, using a 100×/1.49 N.A. oil-immersion objective (Nikon) and selecting a 200-μm pinhole on the same imaging system (Thorlabs). EYFP was excited with a 488-nm laser, fluorescence collected with a 535-nm filter, and three consecutive images were averaged.

Endocytosis Assays. Albumin and transferrin uptake were measured to investigate receptor-mediated endocytosis, and dextran uptake was measured to investigate fluid-phase endocytosis by using modifications of standard methods, as described (14–16). Cells were seeded in 24-well plates and grown for 7 d until polarized. To measure albumin uptake, cells were exposed to 50 μg/mL albumin conjugated to Alexa Fluor 488 (Molecular Probes) for 120 min (13). To measure transferrin uptake, cells were exposed to 50 μg/mL transferrin conjugated to Alexa Fluor 594 (Molecular Probes) for 15 min (13). To measure dextran uptake, cells were exposed to

5 mg/mL dextran conjugated to FITC (Sigma-Aldrich) for 15 min (13). At the end of the uptake period, cells were washed in ice-cold PBS and solubilized in imidazole buffer (1 mM EDTA, 20 mM imidazole at pH 7.2, and 250 mM sucrose). The Alexa Fluor 488, Alexa Fluor 594, and FITC fluorescence was determined by using a CytoFluor microplate reader (PerSeptive Biosystems) at 485-nm excitation and 530-nm emission wavelengths for albumin-488 and FITC-dextran and 596-nm excitation and 615-nm emission wavelengths for transferrin-594, respectively (13). Total Alexa Fluor 488-albumin or Alexa Fluor 594-transferrin uptake was standardized to total cellular protein. For competition experiments, cells were simultaneously incubated with either 5 mg/mL unlabeled albumin or 5 mg/mL unlabeled transferrin during the endocytosis assay, and the uptake of fluorescent albumin or transferrin determined (13). Fluorescence uptake in Dent disease ciPTECs and competition assays was expressed relative to uptake in control ciPTECs without competition. Significance values were calculated by unpaired, two-tailed Student's *t* test.

Acidification Studies. Endosomal pH was determined by using a modification of methods described (17, 18). To generate a standard curve, control ciPTECs were first plated in six-well plates and transfected with pHluorin-glycosylphosphatidylinositol (GPI), which is expressed on the cell surface, using FuGene6 (Roche), and bathed in buffers of differing pH. Fluorescence was imaged in live cells by using a Zeiss LSM510-META confocal microscope 21–23 h after transfection. pHluorin was excited at 488 nm by using a diode laser and at 760 nm by using an argon two-photon laser. Emitted fluorescence was collected through a 505-nm long-pass filter. ImageJ software was used to measure the fluorescence intensity at each wavelength and the 760 nm to 488 nm ratio calculated in each buffer to construct a standard curve (18). To determine endosomal pH, ciPTECs were plated in six-well plates and transfected with pHluorin-vesicle-associated membrane protein (VAMP2), which is expressed at the endosomal membrane. pHluorin-VAMP2–expressing cells were imaged at 488 nm and 760 nm, and the 760 nm/488 nm ratios were compared with the standard curve to determine vesicular pH (18). For bafilomycin experiments, 25 μM Bafilomycin-A1 (Sigma-Aldrich) was applied to the cells and incubated at 37 °C for 1 h before recordings were made. Significance values were calculated by unpaired, two-tailed Student's *t* test.

Electrophysiological Studies. The WT pEYFP–CLC-5 construct (18) was used to generate the His insertion at codon 30 (30:insH) and R637X mutants by site-directed mutagenesis (QuikChange; Stratagene). HEK293 cells were transiently transfected with wild-type or mutant EYFP–CLC-5 constructs by using FuGENE 6 reagent (Promega) and incubated for 2–3 d. Transfected cells were identified by EYFP epifluorescence, and whole-cell currents were recorded at room temperature (20–22 °C) by using an EPC-10 patch clamp amplifier under control of Patchmaster software (HEKA). The bath solution contained 150 mM NaCl, 5 mM KOH, 10 mM Hepes, 2.6 mM $MgCl_2$, 1.2 mM $CaCl_2$, 5 mM glucose at pH 7.4 with NaOH, and patch pipettes (2-3 MΩ) were filled with solution containing 42 mM CsCl, 98 mM aspartic acid, 10 mM EGTA, 10 Hepes, and pH 7.4 with CsOH. Cells were held at −30 mV and 10-ms voltage pulses (P) were applied from −100 to +200 mV. A leak-subtraction protocol, which uses voltage pulses one-quarter of the amplitude and in the opposite polarity to the test voltage pulses (P÷(−4)) to measure the Ohmic membrane properties at voltages below the threshold for CLC-5 activation, was used to subtract residual capacitance and leak currents.

Data were analyzed by plotting the relationship between the current density (steady-state current divided by whole-cell capacitance) and voltage. Conductance density was calculated by dividing the current density by the driving force, V-E_{rev}, where V is the membrane voltage and E_{rev} the calculated reversal potential (of −20.5 mV), and derived by using the $[Cl^-]$ and pH of the solutions and assuming $2Cl^-/1H^+$ exchange transport, as described (18). Recordings were measured in $n = 11$, 10, and 6 cells for WT, 30:insH, and R637X, respectively. Conductance density (G)–voltage (V) relationships from each cell were fitted with a Boltzmann function in the form $G = G_{max}/(1+e^{(V1/2-V)/k})$, where G_{max} is the maximum conductance density of the cell membrane, $V_{1/2}$ the half-maximal activation voltage, and k a factor relating to the steepness of the voltage dependence. Because recordings from cells expressing R637X contained a greater proportion of endogenous HEK293 cell currents, which might distort the measured activation parameters, and because the analysis assumed that $2Cl^-/H^+$ transport is preserved in the mutant CLC-5, an alternative method of measuring relative transporter activity was used. CLC-5 activation was quantified by integrating the inward current recorded upon repolarization to −30mV as a measure of the relative gating charge movement (Q_{OFF}) (19). Charge (Q)–voltage (V) relationships were analyzed by using a similar Boltzmann function, substituting Q for G. Data are expressed as mean ± SEM of number of cells. Comparisons between data and parameters obtained from cells expressing the different CLC-5 variants were compared by using ANOVA and Bonferroni post hoc analysis of individual means. Statistical significance is stated when $P < 0.05$ between individual datasets.

Proton-Transport Function Assessed by Intracellular pH Changes. HEK293 cells were transfected with wild-type or mutant pEYFP–CLC-5 constructs as described above and seeded onto 35-mm Fluorodishes (World Precision Instruments). The same electrophysiological solutions and apparatus were used as above, but 50 μM of the pH-sensitive dye 2′,7′-bis(carboxyethyl)-5(6)-carboxyfluorescein (BCECF; Biotium) was added to the pipette solution. After establishing the whole-cell configuration, cells were held at −30 mV and left for at least 5 min for the BCECF to load into the cell from the patch pipette. Fluorescence was imaged on a Nikon TE-2000 microscope by using a 40× objective lens and a laser scanning imaging system (Thorlabs). Images were collected over 30 s at 1 frame per s, exciting with a 488-nm laser and collected with 535-nm filter. A pinhole of 2 mm was selected to collect images from an optical slice containing the whole cell. Between the 10- and 20-s timepoints, 100-ms voltage pulses to +150 mV were applied at 5 Hz to activate CLC-5. Fluorescence intensity from a region of interest enclosed by the cell was analyzed by using ImageJ software. Data were background subtracted and corrected for bleaching by extrapolating the change in intensity over the first 9 s, which upon inspection was very close to linear. For comparison between cells, fluorescence intensity was expressed as a percentage change relative to baseline.

1. Wilmer MJ, et al. (2010) Novel conditionally immortalized human proximal tubule cell line expressing functional influx and efflux transporters. *Cell Tissue Res* 339(2): 449–457.
2. Racusen LC, Fivush BA, Andersson H, Gahl WA (1991) Culture of renal tubular cells from the urine of patients with nephropathic cystinosis. *J Am Soc Nephrol* 1(8):1028–1033.
3. O'Hare MJ, et al. (2001) Conditional immortalization of freshly isolated human mammary fibroblasts and endothelial cells. *Proc Natl Acad Sci USA* 98(2):646–651.
4. Gil-Bernabé AM, et al. (2012) Recruitment of monocytes/macrophages by tissue factor-mediated coagulation is essential for metastatic cell survival and premetastatic niche establishment in mice. *Blood* 119(13):3164–3175.
5. Lloyd SE, et al. (1996) A common molecular basis for three inherited kidney stone diseases. *Nature* 379(6564):445–449.
6. Bowl MR, et al. (2010) Identification and characterization of novel parathyroid-specific transcription factor Glial Cells Missing Homolog B (GCMB) mutations in eight families with autosomal recessive hypoparathyroidism. *Hum Mol Genet* 19(10):2028–2038.
7. Glasmacher E, et al. (2010) Roquin binds inducible costimulator mRNA and effectors of mRNA decay to induce microRNA-independent post-transcriptional repression. *Nat Immunol* 11(8):725–733.
8. Lemos MC, Harding B, Shalet SM, Thakker RV (2007) A novel MEN1 intronic mutation associated with multiple endocrine neoplasia type 1. *Clin Endocrinol (Oxf)* 66(5):709–713.

9. Wang D, et al. (2006) Antioxidants protect PINK1-dependent dopaminergic neurons in Drosophila. *Proc Natl Acad Sci USA* 103(36):13520–13525.
10. Pfaffl MW (2001) A new mathematical model for relative quantification in real-time RT-PCR. *Nucleic Acids Res* 29(9):e45.
11. Wilmer MJ, et al. (2010) Novel conditionally immortalized human proximal tubule cell line expressing functional influx and efflux transporters. *Cell Tissue Res* 339(2):449–457.
12. Jeong WS, et al. (2005) Differential expression and stability of endogenous nuclear factor E2-related factor 2 (Nrf2) by natural chemopreventive compounds in HepG2 human hepatoma cells. *J Biochem Mol Biol* 38(2):167–176.
13. Reed AA, et al. (2010) CLC-5 and KIF3B interact to facilitate CLC-5 plasma membrane expression, endocytosis, and microtubular transport: Relevance to pathophysiology of Dent's disease. *Am J Physiol Renal Physiol* 298(2):F365–F380.
14. Hryciw DH, et al. (2003) Cofilin interacts with ClC-5 and regulates albumin uptake in proximal tubule cell lines. *J Biol Chem* 278(41):40169–40176.
15. Gekle M, Mildenberger S, Freudinger R, Schwerdt G, Silbernagl S (1997) Albumin endocytosis in OK cells: Dependence on actin and microtubules and regulation by protein kinases. *Am J Physiol* 272(5 Pt 2):F668–F677.
16. Gekle M, Mildenberger S, Freudinger R, Silbernagl S (1995) Kinetics of receptor-mediated endocytosis of albumin in cells derived from the proximal tubule of the kidney (opossum kidney cells): Influence of Ca2+ and cAMP. *Pflugers Arch* 430(3):374–380.
17. Miesenböck G, De Angelis DA, Rothman JE (1998) Visualizing secretion and synaptic transmission with pH-sensitive green fluorescent proteins. *Nature* 394(6689):192–195.
18. Smith AJ, Reed AA, Loh NY, Thakker RV, Lippiat JD (2009) Characterization of Dent's disease mutations of CLC-5 reveals a correlation between functional and cell biological consequences and protein structure. *Am J Physiol Renal Physiol* 296(2):F390–F397.
19. Smith AJ, Lippiat JD (2010) Voltage-dependent charge movement associated with activation of the CLC-5 2Cl-/1H+ exchanger. *FASEB J* 24(10):3696–3705.

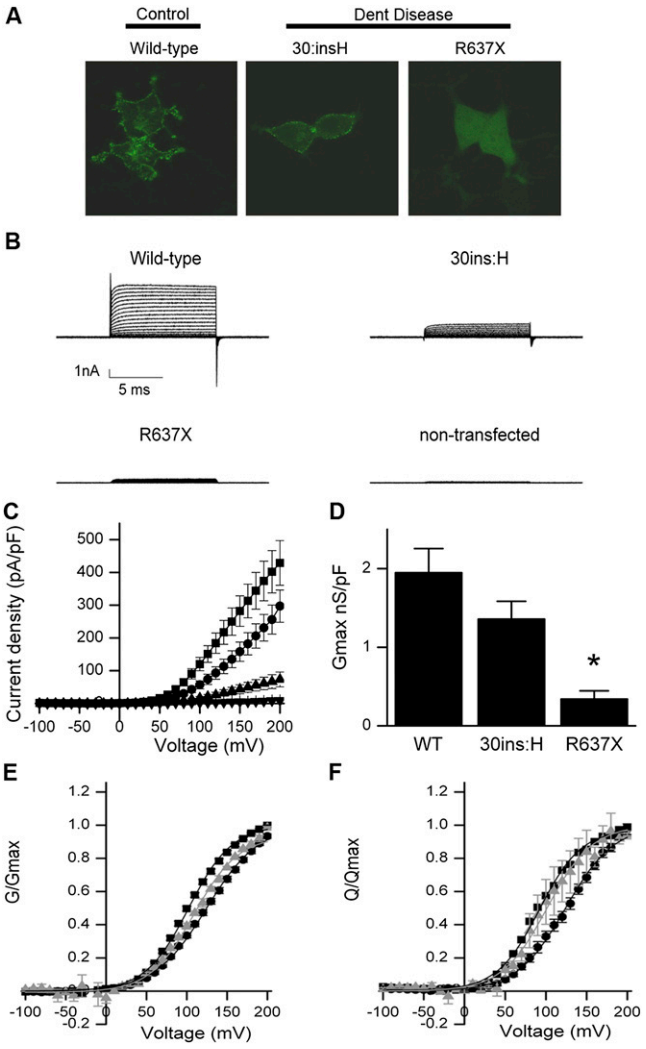

Fig. S1. Electrophysiological studies of CLC-5 mutants. (*A*) Confocal microscopy of HEK293 cells transiently transfected with CLC-5–YFP WT, 30:insH, and R637X constructs to study cell surface expression. The del132-241 CLC-5 mutant was not assessed because no CLC-5 protein was present in the del132-241 ciPTEC (Fig. S3). WT and 30:insH have predominantly cell surface expression, whereas R637X is largely cytoplasmic. Therefore, only those recordings from R637X-expressing cells that had sufficient surface membrane expression to resolve gating currents were included in the analysis of voltage dependence of CLC-5 gating charge. (*B*) Representative whole-cell current families from a HEK293 cell transiently transfected with WT CLC-5 construct, or mutant 30:insH or R637X CLC-5 constructs, and compared with those from a nontransfected cell. Voltage pulses were applied to −100 to +200 mV from a holding potential of −30 mV. (*C*) Mean ± SEM current density–voltage relationship from cells expressing WT (squares, $n = 11$), 30:insH (circles, $n = 10$), and R637X (triangles, $n = 6$) CLC-5 and nontransfected cells (inverted triangles, $n = 3$). Cells expressing either 30:insH or R637X CLC-5 gave currents that were significantly smaller than WT at +100 mV, but only R637X CLC-5 currents were significantly smaller than WT at +200 mV ($P < 0.05$). (*D*) Mean ± SEM maximum current densities (G_{max}) returned from fits of Boltzmann functions to conductance density–voltage relationships. The mean (G_{max}) for R637X was significantly smaller than that for WT CLC-5 (*$P < 0.05$ compared with WT CLC-5). (*E*) Activation curves generated by normalizing current density–voltage relationships to the fitted G_{max}. The activation of voltage dependence for both CLC-5 mutants was significantly shifted to more positive potentials, with half-maximal activation voltages ($V_{1/2}$) of 102 ± 1.7 mV, 125 ± 2.5 mV, and 115 ± 1.8 for WT, 30:insH, and R637X CLC-5, respectively ($n = 6$–11). (*F*) Relative Q_{OFF} currents measured as the charge moved during the transient inward currents recorded at the end of the voltage pulse. To measure this relative transporter activity, integration of the transient inward "tail" current, representative of the conformational change from active to inactive state (19) was performed. The symbols in *E* and *F* representing data from cells expressing WT, 30:insH, and

Legend continued on following page

R637X CLC-5 are the same as those in *C*, and R637X data are shown in gray for clarity. The solid curves in *E* and *F* are Boltzmann functions fitted to mean data and the shifts in half-maximal activation. The voltage dependence of CLC-5 gating charge movement in 30:insH, but not R637X, was significantly shifted to more positive potentials (V_{max} were 94 ± 3.9 mV (n = 11), 124 ± 4.2 mV (n = 10), and 104 ± 14.1 mV for WT, 30:insH, and R637X CLC-5, respectively). The conductance voltage normalized to maximum conductance of the 30:insH mutation shows the $V_{1/2}$max is 25 mV more positive than WT. Thus, the mutant CLC-5 requires a more depolarized cell membrane to obtain equivalent transport activity, which may be responsible for the delayed endocytosis (Fig. 2). The R637X CLC-5 had severe reductions in chloride conductance and cell surface expression compared with wild-type CLC-5, which is likely responsible for the significantly reduced H^+ efflux measured by using BCECF (Fig. S4). Therefore, the combined reduction in cell surface expression, reduced chloride conductance and H^+ efflux are likely responsible for the observed impairments in receptor-mediated endocytosis and megalin trafficking within these ciPTECs.

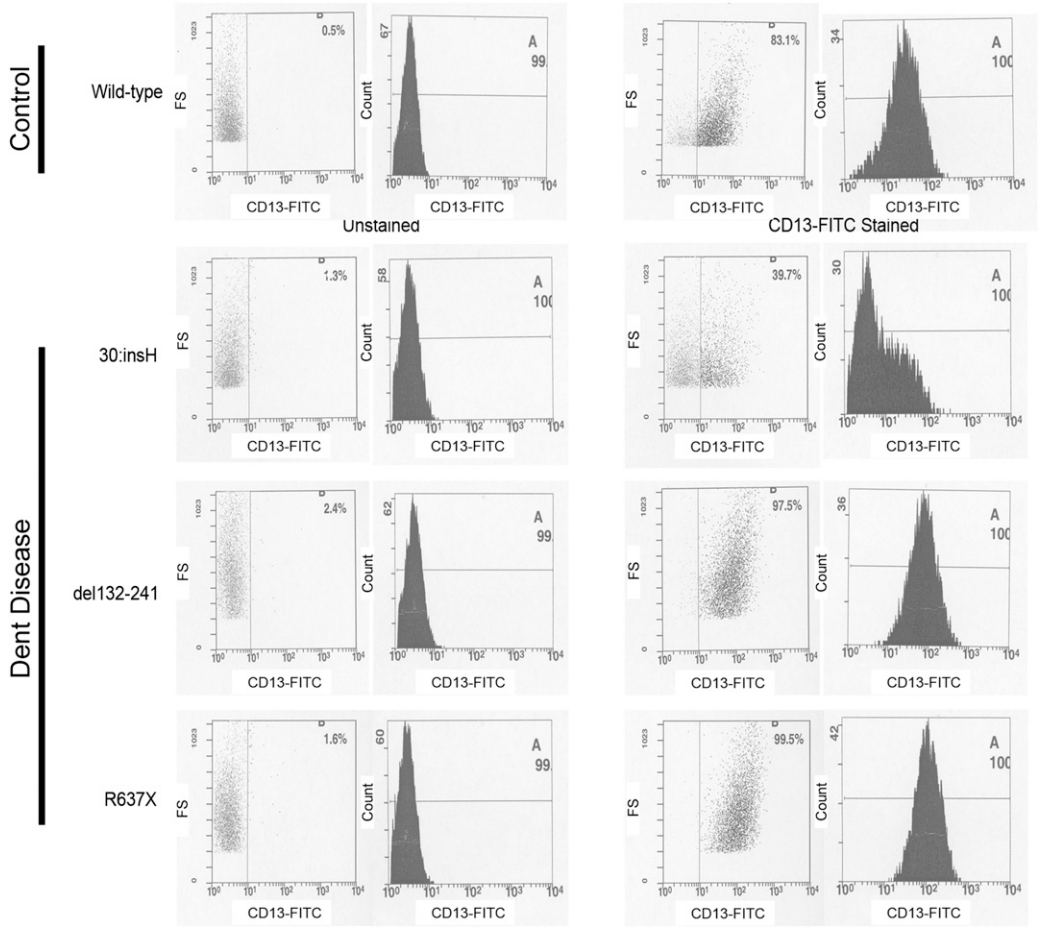

Fig. S2. Examination of Dent disease and control cell lines by flow cytometry. Cells were examined for the presence of the proximal tubular marker CD13 (aminopeptidase-N) by flow cytometry. Readings were initially made in unstained cells, then in CD13-FITC–treated cells. Forward scatter was plotted against CD13-FITC in histograms to compare unstained and stained cells. Cell lines with the mutation 30:insH had mixed cell populations with <45% of cells being CD13-FITC positive. In contrast, the del132-241 and R637X cells were comparable to the control cells with >90% of cells being CD13-FITC positive.

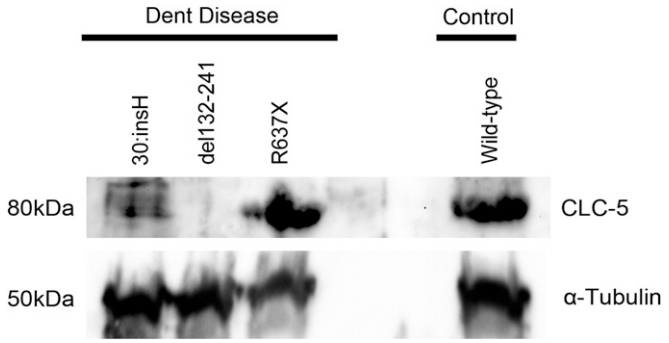

Fig. S3. CLC-5 expression. Western blot analysis of control (wild-type) ciPTEC lysates revealed the presence of the 80-kDa CLC-5 protein. However, CLC-5 expression in the mutant ciPTECs was abnormal compared with wild-type ciPTEC. Thus, CLC-5 protein was markedly degraded in 30:insH ciPTECs, absent in del132-241 ciPTECs, and truncated in R637X ciPTECs. Expression of α-tubulin was used as a control to confirm equal loading of protein.

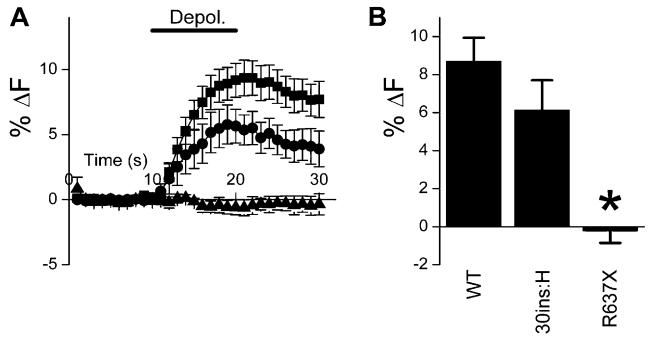

Fig. S4. Changes in intracellular pH following activation of CLC-5 variants expressed at the plasma membrane. HEK293 cells were transiently transfected with a WT CLC-5 construct or mutant CLC-5 constructs that had the mutations 30:insH or R637X. To determine whether the cell surface expressed WT or mutant CLC-5s were capable of supporting H^+ transport, cytoplasmic pH was monitored by measuring BCECF fluorescence loaded from the patch pipette. (*A*) Mean (± SEM) fluorescence intensity measured over 30 s from cells expressing WT (squares, $n = 7$), 30:insH (circles, $n = 7$), and R637X (triangle, $n = 6$) CLC-5. Fluorescence intensity from each cell was normalized to the mean intensity measured over the first 9 s, and data are expressed as percentage change from this baseline (% ΔF). A 10-s train of depolarizing voltage pulses to +150 mV was applied between the 10- to 20-s time points as indicated (Depol.) to drive currents through the CLC-5 variants. (*B*) Peak fluorescence change (average of three consecutive measurements) from the same data presented in *A*. *$P < 0.05$ compared with WT; WT and 30:insH data are not significantly different. These results show that upon application of a 10-s train of depolarizing voltage pulses to +150 mV, the BCECF fluorescence increases in cells expressing WT and 30:insH, but not R637X CLC-5. The increase in fluorescence represents an alkalinization of the cell interior and is consistent with voltage-activated transport of H^+ out of the cell by both WT and 30:insH CLC-5. The results with R637X CLC-5 are likely due to insufficient protein at the plasma membrane (Fig. S1) to support pH change. Measurement of the proton efflux of the 30:insH mutant CLC-5 and wild-type CLC-5 demonstrated them to be similar.

Table S1. *CLCN5* expression detected by qRT-PCR in WT and Dent Disease mutant ciPTECs

ciPTEC		Fold change	*t* test compared with WT
Control	Wild-type	1.00 ± 0.31	—
Mutant	30:insH	0.51 ± 0.06	0.31
	del132-241	0.47 ± 0.14	0.27
	R637X	1.01 ± 0.12	0.98

CLCN5 expression was assessed by qRT-PCR using RNA obtained from control (WT) and Dent disease mutant (30:insH, del132-241, and R637X) ciPTECs. Fold changes are expressed relative to WT levels ($n = 12$, obtained from replicates for each of four biological replicates per ciPTEC). *P* values were calculated by Student's unpaired, two-tailed *t* test.